MODELING AND SIMULATION RESULTS ON HIGH SENSITIVITY SCATTERED GAMMA-RAY IMAGING

Clémence Driol[1], **M. K. Nguyen**[2], **T. T. Truong**[1]

[1]LPTM / CNRS UMR 8089 / Université de Cergy-Pontoise
2 rue Adolphe Chauvin, 95302 Cergy-Pontoise Cedex, France
[2] ETIS / CNRS UMR 8051 / ENSEA / Université de Cergy-Pontoise
6 avenue du Ponceau, 95014 Cergy-Pontoise Cedex, France

cdriol@u-cergy.fr (Clémence Driol)

Abstract

Emission gamma ray imaging is widely used in numerous fields such as medical imaging, non-destructive testing, gamma astronomy and environmental survey. In conventional nuclear imaging, a collimated gamma camera rotates in space to collect primary emitted radiation by an object under investigation. In this case Compton scatter radiation behaves generally as noise hindering image quality and consequently correction to scatter should be applied.
However recently an interesting new imaging concept, which uses precisely scattered radiation by the object medium (instead of primary radiation) as imaging agent, has been advocated. The camera records now images labeled by scattered photon energy or equivalently scattering angle. Then it is shown that the three dimensional image reconstruction from scattered radiation data detected by a conventional collimated camera is feasible [1, 2, 3, 4]. However, the image sensitivity is considerably low because of the presence of the collimator. Therefore in order to record a larger amount of scattered radiation, we extend the working of the previous imaging principle to a camera without collimator. But this move brings up new computational difficulties due to summations over allowed directions entering the detector.
A novel analysis of photon propagation from emission to detection is modeled and validated by Monte-Carlo simulations. This permits to compare signals received by a camera with or without collimator. Then, we show results of two dimensional numerical reconstruction of the object radiation activity from simulated scattered radiation recorded by an uncollimated camera. These encouraging results are a necessary step before a future extension to three dimensional imaging.

Keywords: Biomedical imaging modeling, Sensitivity, Monte-Carlo simulations

Presenting Author's Biography

Clémence Driol graduated in 2005 from the Ecole Nationale Supérieure de Physique de Strasbourg, France, in photonic engineering. She is currently working on a PhD thesis at the University of Cergy-Pontoise, France. Her research interest is in the fields of the scattered gamma ray imaging, optical imaging, inverse problems, Monte-Carlo simulation.

ISBN 978-3-901608-32-2

1 Modeling of two dimensional image formation

We establish first the radiation propagation in a two-dimensional (2D) slice (thin section) of a scattering medium. The medium electronic density n_e is assumed to be approximately constant and attenuation will be neglected in this first part.

Let
- $\mathbf{S}$ be a radiation emitting point source of an object described by its activity density $f(\mathbf{S})$ (number of photons emitted per unit time), assumed to be isotropic,
- $\mathbf{M}$, a scattering site in the medium,
- $n_e(\mathbf{M})$, the electron density at site $\mathbf{M}$,
- $\mathbf{D}$, a detection site on a linear detector which collects the photon flux density at a photon energy E_ω (see Eq. (1)).

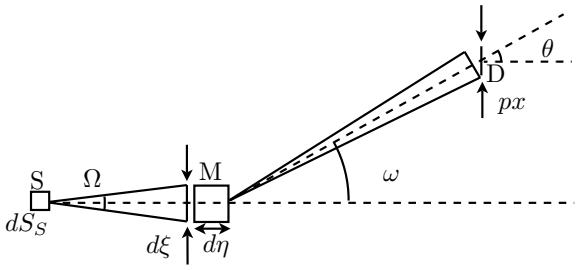

Fig. 1 Geometry of a Compton scattering: source site $\mathbf{S}$, scattering site $\mathbf{M}$, detection site $\mathbf{D}$ of length px

The energy of scattered photon is related to the scattering angle ω by the Compton relation:

$$E_\omega = E_0 \ \frac{1}{1+\sigma(1-\cos\omega)}, \qquad (1)$$

where E_0 is the emitted photon energy, $\sigma = E_0/mc^2$ and mc^2 the rest energy of the electron.

From Fig. 1, one can see that the photon flux density reaching a site $\mathbf{M}$ is the number of photons emitted into the angular fan Ω per unit length and per unit time:

$$\frac{f(\mathbf{S})d\mathbf{S}_S}{2\pi} \ 2\arctan\left(\frac{d\xi}{2\,|SM|}\right) \ \frac{1}{d\xi}, \qquad (2)$$

where $|SM|$ is the distance between sites $\mathbf{S}$ and $\mathbf{M}$ and $d\mathbf{S}_S$ the area element around $\mathbf{S}$. The fraction of photons scattered in the direction making an angle ω with the incident direction depends on the Compton differential cross section $\sigma_S^C(\omega)$ (which has the dimension of a length in 2D) and on the number of electrons $n_e(\mathbf{M})\ d\mathbf{S}_M$ at site $\mathbf{M}$, $d\mathbf{S}_M$ being the integration area element around $\mathbf{M}$. Hence the scattering photon flux density received at the detection site $\mathbf{D}$ is given by :

$$d\phi(\mathbf{D},\omega|\mathbf{S}) = \frac{f(\mathbf{S})d\mathbf{S}_S}{2\pi} \ 2\arctan\left(\frac{d\xi}{2\,|SM|}\right) \ \frac{1}{d\xi}$$

$$n_e(\mathbf{M})\ d\mathbf{S}_M \ \sigma_S^C(\omega) \ 2\arctan\left(\frac{px}{2\,|MD|}\right) \ \frac{1}{px} \ \cos\theta, \qquad (3)$$

where θ is the angle between the outgoing unit vector and the detector normal to the photon incident direction, $|MD|$ the distance from scattering site $\mathbf{M}$ to detection site $\mathbf{D}$. In fact there will be two scattering sites $\mathbf{M}_1$ et $\mathbf{M}_2$ as shown in Fig. 2.

The total photon flux density at a site $\mathbf{D}$ is the integral over all source sites and all scattering sites such that the scattering angle is ω. This constraint is expressed by a δ-function as follows :

$$g(\mathbf{D},\omega) = \int\int d\phi(\mathbf{D},\omega|\mathbf{S})\,\delta(\widehat{SMD}-(\pi-\omega)), \qquad (4)$$

where $\widehat{SMD}$ is the angle at vertex $\mathbf{M}$ of the triangle SMD (see Fig. 2).

2 Computation of the image of a point source

The Point Spread Function (PSF) is by definition the image of a single point source at site $\mathbf{S}$ and of intensity f_0. Eq. (4) can be rewritten in terms of the PSF as follows :

$$g(\mathbf{D},\omega) = \int d\mathbf{S}_S \ \ f(\mathbf{S}) \ \ PSF(\mathbf{D},\omega|\mathbf{S}). \qquad (5)$$

For a camera without collimator, the scattering sites due to a single point source $\mathbf{S}$ are located on two circular arcs subtending an angle $(\pi-\omega)$ (Eq. (4)). The photon flux density received at site $\mathbf{D}$ is then given by an integration over these two circular arcs (see Fig. 2).

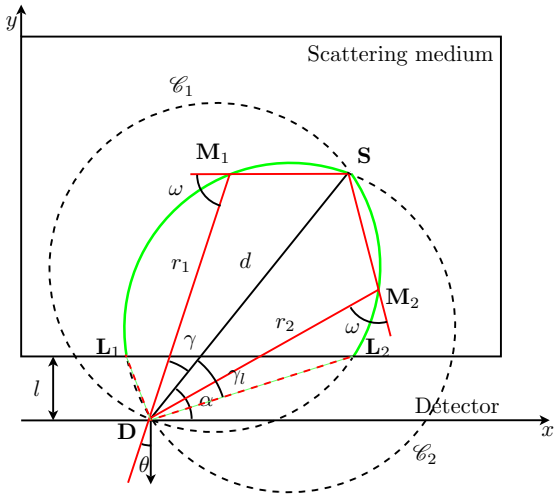

Fig. 2 Scattering sites contributing to detection site D without collimator (green or full line circular arcs)

For computation we use polar coordinates (r,γ), such that $\mathbf{S} = (d,\alpha)$ with $DS = d$ and $\mathbf{M} = (r,\gamma)$, with $DM = r$ and $\overrightarrow{DM}\cdot\overrightarrow{DS} = r\,d\,\cos\gamma$.

The circular arcs have polar equations:

$$r = d\,\frac{\sin(\omega-\gamma)}{\sin\omega} \qquad \text{and} \qquad r = d\,\frac{\sin(\omega+\gamma)}{\sin\omega}, \qquad (6)$$

ISBN 978-3-901608-32-2

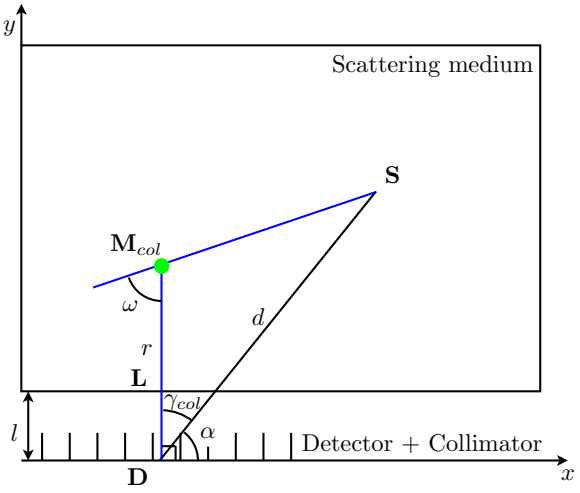

Fig. 3 Single scattering site contributing to detection site D with collimator (green spot)

where γ is the angle between $\overrightarrow{DS}$ and $\overrightarrow{DM}$. The distance $|SM|$ can be extracted from a simple identity in the triangle DSM:

$$|SM| = d\ \frac{\sin\gamma}{\sin\omega}. \tag{7}$$

And the integration area $d\mathbf{S}_M$ is now reduced to the arc element:

$$d\mathbf{S}_M \rightarrow \sqrt{dr^2 + r^2 d\gamma^2} = \frac{d}{\sin\omega}\ d\gamma. \tag{8}$$

Hence the PSF is given by the sum of the two integrations on γ:

$$PSF(\mathbf{D},\omega|\mathbf{S}) = \frac{K(\omega)\,d}{d\xi\ px\ \sin\omega} \sum_{2\ \text{Arcs}} \int_0^{\gamma_l(\omega)} d\gamma\ \cos\theta(\gamma)$$

$$\arctan\left(\frac{d\xi}{2d}\frac{\sin\omega}{\sin\gamma}\right)\ \arctan\left(\frac{px}{2d}\frac{\sin\omega}{\sin(\omega\pm\gamma)}\right), \tag{9}$$

where $K(\omega) = 4n_e\sigma_S^C(\omega)f_0/2\pi$, $\cos\theta = \sin(\alpha-\gamma)$ if the detector lies along the $0x$ axis and l is the distance between the line detector and the linear lower boundary of the medium. The integration is carried out over the points inside the scattering medium. Therefore when the medium is of finite extent, the limit of the integration $\gamma_l(\omega)$, which corresponds to the intersection of the arc of circle with the scattering medium, should be calculated beforehand, see Fig. 2.

Now if the collimator is mounted on the detector, then only one scattering site $\mathbf{M}$, located on the perpendicular to the detector at site $\mathbf{D}$, will contribute to detection site $\mathbf{D}$, (see Fig. 3). Thus the integration on γ is restricted by a delta function which picks out only the corresponding value of γ, i.e.:

$$\gamma_{col} = \frac{\pi}{2} - \alpha. \tag{10}$$

The resulting PSF expression for a collimated detector is:

$$PSF_{col}(\mathbf{D},\omega|\mathbf{S}) = \frac{K(\omega)\,d}{d\xi\ px\ \sin\omega}$$

$$\arctan\left(\frac{dx}{2d}\frac{\sin\omega}{\cos\alpha}\right)\ \arctan\left(\frac{px}{2d}\frac{\sin\omega}{\pm\cos(\alpha\mp\omega)}\right). \tag{11}$$

3 Comparison between PSF modeling and Monte-Carlo simulations

A 256 pixels detector is placed on the $0x$ axis. The pixel size is 0.11×0.11 mm^2. The scattering medium is a rectangular sheet of dimensions 30 cm $\times$ 15 cm $\times$ 0.11 mm, which is at a distance of 1 cm above the linear detector. Since biological tissues have an electronic structure close to that of water, we shall take $n_e = 3.34\times10^{23}$ electrons/cm^3.

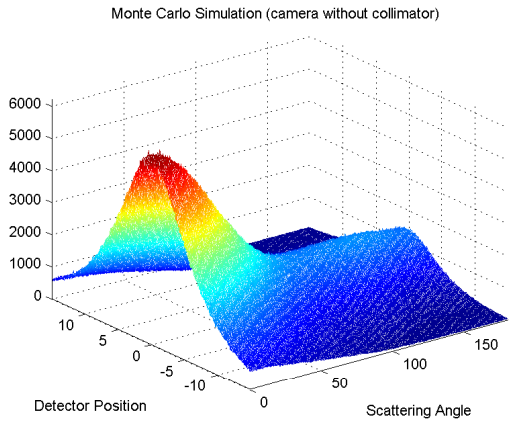

Fig. 4 First order Monte-Carlo simulation of PSF for a camera without collimator

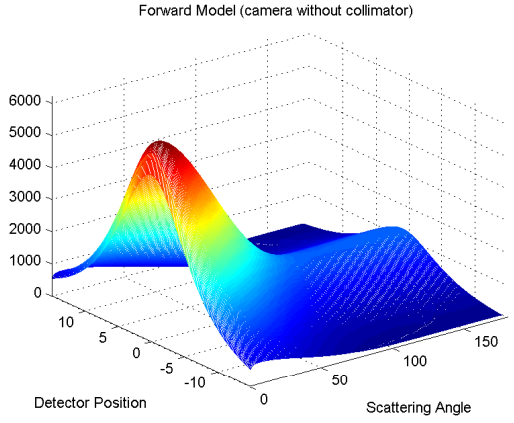

Fig. 5 Forward Model of PSF for a camera without collimator

A point source is placed in the scattering medium at 6 cm above the detector. The radio pharmaceutical used in this simulation is medical Technecium 99, which emits photons with energy 140.1 keV. The activity density of the source is about $27 \times 10^{-3} Ci/cm^3$, with an acquisition time per image of one second (see Fig. 9).

In order to check the validity of the previous forward model, we have carried out Monte-Carlo simulations. In this process, the medium attenuation is due mainly to the sum of photoelectric absorption and Compton scattering at energies of 90 keV to 140 kev (see Tab. 1 [5]). The validation of the forward model consists in doing on one hand the comparison with a Monte-Carlo simulation of order one, i.e. allowing only a single scattering, and on the other hand, in evaluating the discrepancy with a Monte-Carlo simulation allowing multiple scattering.

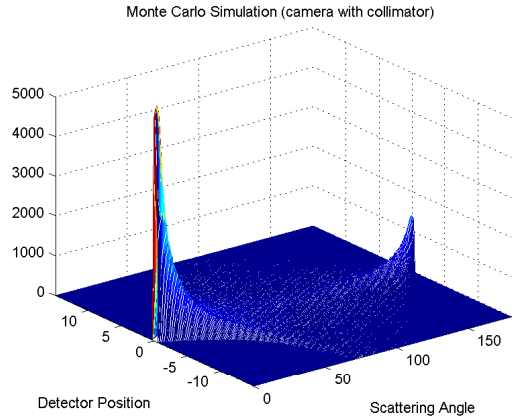

Fig. 6 First order Monte-Carlo simulation of PSF for a camera with collimator

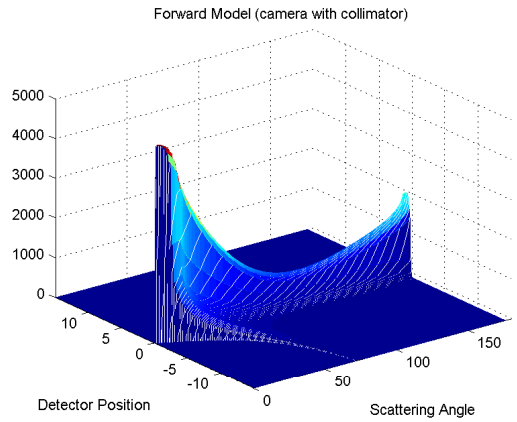

Fig. 7 Forward Model of PSF for a camera with collimator

For this purpose, an attenuation coefficient must be introduced into the forward model (Eqs. (9) and (11)):

$$PSF = \frac{K(\omega)\, d}{d\xi\ px\ \sin\omega} \sum_{2\ \text{Arcs}} \int d\gamma\ \cos\theta\ e^{-\mu_0 |SM|}\, e^{-\mu_\omega |ML'|} \times \arctan\left(\frac{d\xi}{2d}\frac{\sin\omega}{\sin\gamma}\right) \arctan\left(\frac{px}{2d}\frac{\sin\omega}{\sin(\omega \pm \gamma)}\right), \tag{12}$$

where μ_0 and μ_ω are the attenuation coefficients at energies E_0 and E_ω, and $|ML'|$ is the distance from site $\mathbf{M}$ to site $\mathbf{L}'$, intersection of the line MD with the horizontal line $y = l$, representing the medium lower limit, see Fig. 2. The integration is then performed numerically.

Figures 4 and 6 show results of first order Monte-Carlo simulations. We represent the number of photons registered by the detector as a function of the scattering angle (degrees) and the detector position (cm). The relative error for the PSF without collimator between the first order Monte-Carlo simulation and our forward model is 0.15%. For the PSF with collimator, this error is 1.54%.

Now at a fixed scattering angle ω, the PSF curve as function of the detector position with collimator has a Mexican hat shape while the PSF curve without collimator has a wide Lorentzian shape. On the whole, the detector without collimator collects about 12 times more photons than with collimator, see Fig. 8.

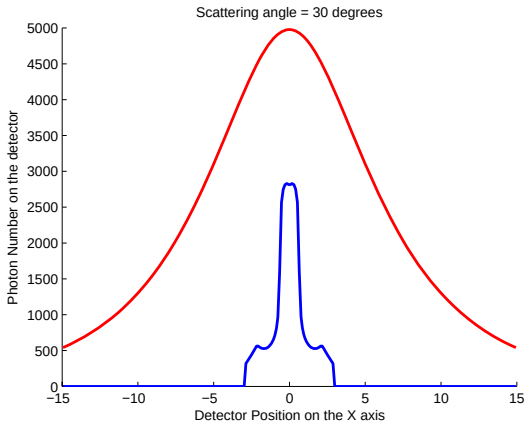

Fig. 8 Comparison of PSF images for a scattering angle of 30° on a detector line: with collimator (blue line) and without collimator (red line)

4 Numerical Reconstruction Results

As an illustration on the possibility of using a uncollimated camera, we carried out two numerical reconstructions: we present first the reconstruction of the single point source from the Monte-Carlo simulated data, and then show the reconstruction of the Shepp-Logan medical phantom from data computed with our model.

4.1 Numerical Point Source Reconstruction

The scattering medium is discretized with 55 points in $0x$ axis direction and with 28 points in $0y$ axis direction.

Energies	Attenuation Coefficient	Scattering Coefficient	Absorption Coefficient
140	0.1538	0.1511	0.0028
120	0.1614	0.1574	0.0040
100	0.1706	0.1646	0.0060
80	0.1833	0.1728	0.0105

Tab. 1 Linear attenuation coefficients for water (cm^{-1})

The detector is reduced to 86 pixels, each one distant from the next by 0.35 cm. We keep the same pixel size as in the section 3. The detector records 86 images of photon energies from 139.6 keV to 90.5 keV. The single point source is centered at 6 cm above the detector (see Fig. 9).

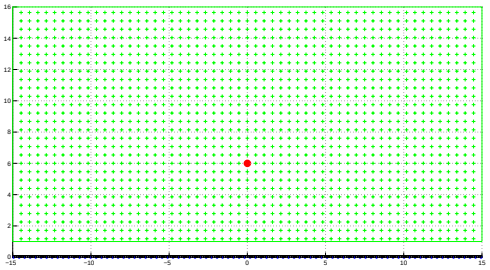

Fig. 9 Point source-medium configuration

We construct the two weight matrices of the medium by calculating from our models (with and without collimator), for each point of the mesh, the PSF at the different scattering angles. The size of the two weight matrices is 7310×1540. This large number of equations compared to the number of unknowns reduces the conditional number (3.10^4 for camera with collimator and 17.10^5 for camera without collimator).

We use the Monte-Carlo simulated gamma-ray data detected by a camera with or without collimator for the reconstruction. The reconstruction is carried out by using the Conjugated Gradient method with positivity constraint.

In the two cases, the source activity is faithfully reconstructed (about 10^9 photons per second). In the case of a camera without collimator, the reconstruction gives a correct side position but produces a vertically lengthened source. The Conjugated Gradient method gives an acceptable reconstruction with 15 iterations, and must be regularized by limiting the number of iterations. Fig. 10 corresponds to 50 iterations.

When the collimator is removed, the reconstruction gives a wider source but the Conjugated Gradient method provides correct results even for a large iteration number. Fig. 11 corresponds to 500 iterations.

4.2 Numerical Image Reconstruction Results

The object is an 2D original Shepp-Logan medical phantom, representing the activity density of the object

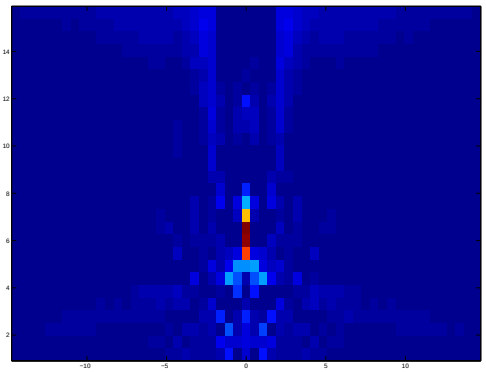

Fig. 10 Point source reconstruction from Monte-Carlo simulated images from a camera with collimator

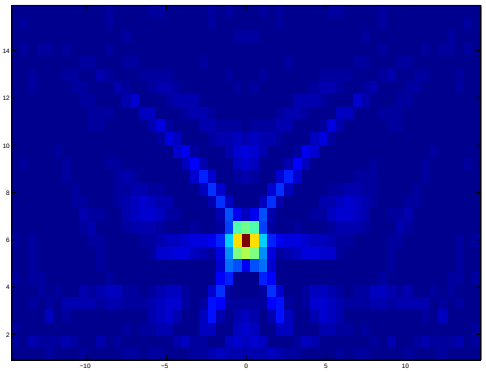

Fig. 11 Point source reconstruction from Monte-Carlo simulated images from a camera without collimator

(see Fig. 12). It is placed at the center of the scattering medium and a unit distance above the detector (Fig. 12). A line detector of 55 pixels of 1 unit length, placed on the axis $y = 0$, is simulated. We consider that the scattering medium has the same attenuation characteristics as water. It consists of a discretized square of 55 $\times$ 55 elements of unit area.

A series of 55 views of the object corresponding to 55 different scattering angles ($12° < \omega < 132°$) have been simulated. Images without collimator are on the average 23 times more sensitive than those with collimator. We construct the 3025 $\times$ 3025 weight matrix by computing, for each mesh point source, the PSF at the

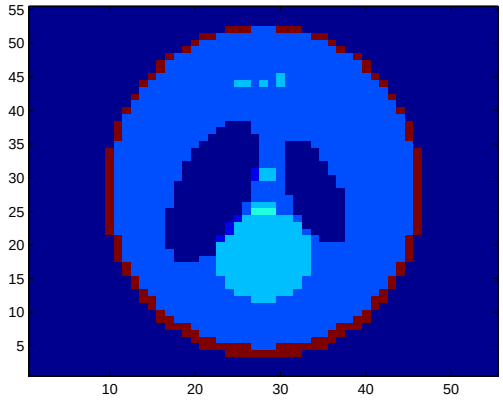

Fig. 12 Original Shepp-Logan phantom

different scattering angles for each site on the detector. The reconstruction is carried out by inverting the weight matrix using the Singular Value Decomposition method, which is less time consuming as compared to the conjugate gradient method.

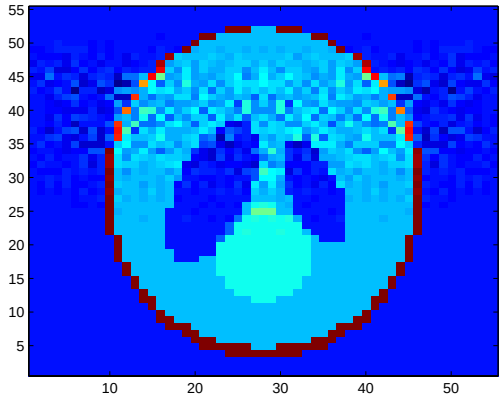

Fig. 13 Shepp-Logan phantom reconstruction with collimator

Fig. 13 and fig. 14 show the reconstruction results with and without collimator. One observes a better agreement with the original object when the collimator is removed. In this case, the relative error is $4.8\ 10^{-7}\%$ instead of 0.08% when the collimator is mounted.

5 Conclusion

These results show the feasibility of image reconstruction using Compton scattered rays detected by a camera without collimator, operating in a fixed position. This is the essence of a new concept of high sensitivity imaging system, which takes advantage of scattering rays instead of rejecting them as done usually. Work aiming at extension to 3D imaging is in progress. The modeling and simulations of multiple scattered radiation are the subject of future investigations.

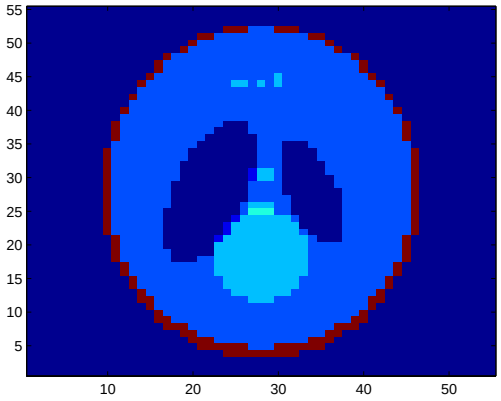

Fig. 14 Shepp-Logan phantom reconstruction without collimator

6 Acknowledgement

The authors thank Dr D. Foster for discussions on Monte-Carlo method.

7 References

[1] M.K. Nguyen and T.T. Truong. On an integral transform and its inverse in nuclear imaging. *Inverse Problems*, 18:265–277, 2002.

[2] M.K. Nguyen, T.T. Truong, J.L. Delarbre, and N. Kitanine. Three dimensional object reconstruction from compton scattered gamma ray data. In Milan Sonka, Ioannis Kakadiaris, and Jan Kybic, editors, *Computer vision and mathematical methods in medical and bio-medical image analysis*, pages 24–34. Springer Verlag, Heidelberg, 2004.

[3] M.K. Nguyen, T.T. Truong, H.D. Bui, and J.L. Delarbre. A novel inverse problem in gamma-ray emission imaging. *Journal of Inverse Problems in Science and Engineering*, 12:225–246, 2004.

[4] J. L. Delarbre, M. K. Nguyen, T. T. Truong, and J. L. Starck. Modeling and simulation for scattered gamma-ray imaging. In *Proc. 5th EUROSIM Congress on Modelling and Simulation*, Marne la Valle, France, September 2004.

[5] http://physics.nist.gov/PhysRefData/XrayMassCoef.

